Deciphering the signatures of convective rain cells using simultaneous observations from C-band Synthetic Aperture Radar onboard EOS-4 satellite and GPM measurements

Kandula V Subrahmanyam, Rajashree V Bothale, M. Swapna and

Prakash Chauhan

Earth and Climate Sciences Area (ECSA),

National Remote Sensing Centre (NRSC), Indian Space Research Organisation (ISRO),

Hyderabad, India-500037

E-mail: kvsm2k@gmail.com; subrahmanyam_kv@nrsc.gov.in

Abstract

Earth Observation Satellite (EOS)-04 launched on 14th February 2022, carries a C-band Synthetic Aperture Radar (SAR) for Agriculture, Forestry, Hydrology and Flood mapping applications. In this paper, we have used C-band SAR images and near-simultaneous observations from the Global Precipitation Measurements (GPM) to study the signatures of multiple convective rain cells. The bright patches are found on C-band SAR imagery, which depicts the information of hydrometeors such as graupels or hails in the melting layer. For the first time, unambiguously estimated the diameter of the convective core rain cells from the C-band SAR backscattered signal and compared near-simultaneous observations from GPM-GMI and Ku-band radar to confirm our findings. In future, we will decipher between convective and stratiform rain signatures on C-band SAR imagery and the possibility between C-band

backscattered signals with lighting events. Thus, the present study demonstrates the potential of C-band SAR for the signatures of convective rain cells.

Keywords: EOS-4, C-band SAR, GPM, convective rain cells, melting layer

1. Introduction

Convective clouds produce a significant amount of precipitation and play a key role in the hydrological cycle (Arakawa, 2004). They further modulates the circulation on regional as well as global scales by releasing the latent heating of energy into the atmosphere (e.g., Reihl and Malkus, 1958; Subrahmanyam and Kumar, 2020). Convective clouds organized into more convective rain cores characterized by strong updrafts and their cloud tops are reaching to tropopause level, where it diverge and spread over the large areas by formation of anvils. In general, tropical convective systems consist of convective core rain cells, which are heavy rainy regions of convective clouds. Further, group of convective clouds produces mesoscale convective systems, which consist of multiple of convective rain cores. The early studies have documented the signatures of tropical convective rain cell on synthetic aperture radar (SAR) images (e.g., Fu and Holt, 1982). Since, then there have been many studies on the footprints of rain cells on SAR images (Fu and Holt, 1982; Jameson et al., 1997; Melsheimer et al., 1998; Alpers et al., 2016 and references therein). SAR is a form of active microwave powerful remote sensing instrument, producing very high-resolution imagery of the Earth's surface in any weather condition (e.g., Melsheimer et al., 1998). With the rapid advancement in technology, the SAR monitoring of Earth is potentially increased by improving the spatial resolutions, revisiting times,

swath width, new processing algorithms, and its polarimetric capability. SAR data has been widely used worldwide in environmental monitoring, Earth resources mapping and military application (e.g., Ouchi, 2013; Alpers et al., 2016). Traditionally, in Earth observation satellites, passive optical sensors in the visible, infrared, thermal and microwave spectrum regions produce the Earth's imagery, but SAR transmits pulses of microwave signal at a fixed wavelength (L-, S-, C- and X-band) and can pierce through clouds to visualize the Earth's surface regardless of atmospheric conditions (e.g., Jameson et al., 1997; Melsheimer et al., 1998). The potential applications of SAR to monitor the melting sea ice, land subsidence, snow cover, deforestation, droughts and floods, wildfires, wetlands, etc., are very useful for assessing and responding to climate change, natural disasters, ecosystem loss, etc. (e.g., Danklmayer et al., 2009).

In addition to the above applications, SAR measurements are utilized in mapping other ocean and atmospheric phenomena such as oceanic fronts, marine atmospheric boundary layer and convective rain cells, which affect the SAR signal (e.g., Fu and Holt, 1982). However, the signature of convective rain is exhibited differently with varying SAR operating frequencies. During heavy rainfall conditions, SAR signal gets attenuated by raindrops in the atmosphere. It is well known that the signature of rain cells can be detected on SAR images at all radar frequencies. Negative impacts of rain for L-band SAR is attributed to wave damping and for X-band increased in SAR signal is observed due to ring waves as well as from the volume scattering (e.g., Melsheimer et al., 1998; Alpers et al., 2016). It becomes more complex, especially at the C-band wavelength, where it lies in the transition region of Bragg scattering (Barren and Gade, 2006). This kind of information on the convective rain cells over the oceanic region is important, where the traditional ground-based weather radars can not observe due to

their range limitation over the oceanic regions. Further, SAR provides high-spatial resolution images, which contain the convective rain signatures providing finer spatial structures of heavy rain events. Combining the SAR observations along with the space borne precipitation simultaneous (e.g., TRMM-precipitation radar, Global Precipitation Measurements (GPM)), will provide better understanding about the convective rain events, which are an alarming rate in the warming climate scenario. Thus, the present study utilizes the C-band SAR data aboard Earth Observation Satellite (EOS)-4 for deciphering the signatures of convective rain events. Also, we used GPM measurements for confirming the rain signatures on C-band SAR images. The technical details about the C-band SAR, GPM satellite and methodology are discussed in Section 2. Section 3 describes the results and discussion of the convective rain events observed by SAR and GPM measurements. Section 4 summarises the results and future scope.

2. Data and methodology

In the present study, we have used C-band SAR backscattering measurements to observe the signatures of convective rain cells. We have used near-simultaneous observations from GMI and Ku-band precipitation radar onboard the GPM satellite to confirm the occurrence of rain cells. This section describes the C-band SAR and GPM data collection and it's processing.

2.1 C-band SAR data processing

C-band SAR onboard Earth Observation Satellite (EOS)-04 satellite was launched on 14 February 2022 by the Indian Space Research Organisation (ISRO). This satellite is in a sun-synchronous orbit at an altitude of 529 km and is a follow-on mission to RISAT-1. The operating frequency of SAR is 5- 5.35 GHz and is variable. The scanning technique of SAR is side-looking, both to left-and-right with 20^{o} - 49^{o} off-nadir. SAR operates in various modes such as High Resolution Spotlight (HRS), Fine Resolution Stripmap (FRS), Medium Resolution ScanSAR (MRS), and the Coarse Resolution ScanSAR (CRS) mode. The resolution of each SAR pixel is 1 m to 50 m, depending on the operation mode. Table 1 provides the more detailed characteristics of various operation modes of C-band SAR. The data used in the present analysis consist of CRS mode, which has the pixel resolution of 50 m. The SAR collects the backscattered signal from the hypothetical stationary Earth's surface as it moves along track. The integration of SAR depends on the synthetic aperture. The longer the synthetic aperture is, the larger the integration. The final resolution of the SAR image is a function of the viewing angle and so-called integration angle, which makes the SAR resolution independent of the distance from the Earth's surfaces. The SAR image data was downloaded from the Bhoonidhi portal (https://bhoonidhi.nrsc.gov.in/bhoonidhi/index.html#). The processing of C-band SAR radiance data over the convective rain cells have been performed and estimated the σ_0 as shown in below equation,

$$\sigma_0=10*\log_{10}(Rad^2-N)+10*\log_{10}(\text{Sin }(I_a))-C$$

Where, σ_0 (dB) is the backscattering coefficient, Rad is the radiance available in the product for different polarizations, N is the image noise bias, I_a is the per pixel incidence angle, and C (dB) is the calibration constant for different polarizations available in the META data file.

2.2 GPM Data

To confirm the convective rain features observed by C-band SAR image, near-simultaneous observations from the Global Precipitation Measurements (GPM) Microwave Imager (GPM-GMI) and Ku-band precipitation radar are used to study the vertical and horizontal structures of convective rain cells. The GPM consist of GMI and dual precipitation radar (DPR) of Ku- (13.6 GHz), and Ka-band (35.5 GHz). The swath width of GMI is 885 km and is used to confirm the spatial pattern of convective rain cells as observed by C-band SAR. The Ka-band is sensitive to light to moderate rainfall, while Ku-band is more sensitive to moderate to heavy rainfall. The swath width of Ku (Ka)-band is 240 (120) km, and the range resolution is 250 m. The minimum resolution for Ka (Ku) -band is 0.2 (0.5) mm/hr (Hou et al., 2014). In the present study, we have used level 2A DPR product (https://storm.pps.eosdis.nasa.gov/storm/), which contains the vertical profiles of Ku- and Ka-band radar data to study the vertical structure of convective rain cells and their horizontal width. This data product also contains information on the melting layer. Results and discussions are discussed in the next section.

3. Results and discussions

Figure 1(a) shows an EOS-4 C-band SAR image acquired on 30 May 2022 over the Australian coast at 1017 UTC, and the zoomed picture of Figure 1(a) is shown in Figure 1(c) in ascending orbit with HV polarization mode. HV denotes that the signal is emitted at horizontal polarization and received at vertical polarization. The white patches are the signatures of the convective rain cell footprints. Figure (b) shows the pass of GPM GMI over the exact location, and the zoomed one is shown in Figure (d), where it is clearly evident that the rain band has multiple convective systems and the maximum rain rate found to be above 30 mm/hr. Further, we have utilized the GPM Ku-band precipitation radar measurements to examine the vertical extent of convective systems. Figure 2(a) depicts the spatial structure of reflectivity at 2km height level. It shows the presence of packets of high reflective areas, which correspond to multiple rain core regions. The bright areas on C-band SAR have almost the same locations in GPM precipitation radar reflectivity observations and correspond to GPM reflectivity higher than 40 dBZ. Therefore, this suggests that the C-band SAR backscattering signal increases at higher rain rates. Melshmeimer et al. (1998) also observed a similar feature with ground-based weather radar (NEXRAD) reflectivity in the convective storm along with a C-band SAR image. The maximum reflectivity is found to be around 50 dBZ (Figure 2). The vertical structure of reflectivity corresponds to the solid line of AB in Figure 2(a) is shown in Figure 2(b). In the present case, the vertical extent of the convective rain cell was found to be around 16.5 km, and the diameter of the convective rain cell is ~ 22 km. In general, the diameter of the convective rain core was around 30 km (e.g., Mapes and Houze, 1995). Further, we have also estimated the diameter of the convective rain cell using a C-band SAR image, as shown in Figure 3. Figure 3(a) shows the spatial distribution

of σ_0 (dB) and (b) shows the various cross-sections of rain cells, which correspond to solid lines in Figure 3(a). From these line profiles, it is evident that the C-band SAR backscattered signal is increased in the presence of convective rain cells, while at L-band, radar signatures consist of dark patches (Alpers et al., 2016). But, in the present case, there is no dark patch visible on the right to the bright patch (Figure 3(a)). In general, the dark areas followed by the bright areas on C-band SAR happened due to the shadowing of the precipitating convective system (Fun and Holt, 1982). From the previous studies (e.g., Alpers et al., 2016; Melshmeimer et al., 1998; Xu et al., 2015) it is assumed that the physical processes which contribute to the signatures of rain over the ocean on SAR image is the scattering of hydrometeors which modifies the sea surface roughness, which increases in the presence of downdraft by hydrometeors often associated with precipitating convective systems, scattering from raindrop splash on the water surface, and volume scattering and attenuation by hydrometeors in the precipitating convective systems. Previous studies also showed that the signatures of convective rain core regions are often not escorted by dark areas on the C-band SAR images (e.g., Fu and Holt, 1982; Melsheimer et al., 1998; Alpers et al., 2016). The bright patches on the C-band SAR image are caused by the reflections of hydrometeors in the melting layer (e.g., Alpers et al., 2016).

In the present case, we have also observed the melting layer from the GPM Ku-band radar measurements, as seen in Figure 2(b & c). Asterisk symbol denotes the melting layer height, which causes a strong backscattered radar signal and is often associated with heights of tropical convective systems at around 4-6 km. The melting layer consists of irregular hydrometeors such as ice/snowflake particles undergoing a phase transition from solid to liquid. In general, the melting layer, also called as ‘bright band’ phenomenon in radar meteorology shows up as higher

reflectivity at the zero-degree isotherm level (Houze, 1997). The main reason for the higher reflectivity in the radar signal (Figure 2 b&c) is that the diameter of falling ice/snowflakes are large but coated with liquid, which has the high refractive index compared to ice, thus shows the high reflectivity values near the melting layer as seen in Figure 2 b &c. In the present case, the height of the melting layer was found to be around 4.8 km. The radar reflectivity in the melting layer showed an enhancement due to the high reflectivity of snow or ice (Houze, 1997), also called a bright band. The stratiform region in the convective system is unambiguously identified by the bright band, as seen in Figures 2(b & c). Thus, the bright patches caused by reflection are not followed by dark areas in the look direction of the C-band SAR antenna, as shown in Figure 1(b). Most of the previous studies interpret the bright patches on C-band SAR images associated with a melting layer due to the non-availability of weather radar observations or other sensors to observe the melting layer independently. Thus, the present study unambiguously demonstrated that the bright regions on the C-band SAR image is due to the presence of a melting layer, which is confirmed by the GPM Ku-band precipitation radar measurements. Alpers et al. (2016) observed a strong reflection of hydrometeors in the melting layer on the SAR images. The example shown in Figure 1 is in HV polarization, which seems to be strongly associated with SAR backscattered signal from hydrometeors in the melting layer than in HH mode (figure not shown). Browne and Robinson (1952) found more contribution from the melting layer by analyzing the radar cross-polarized backscattered signal, and sometimes, they could detect the melting layer signature only at cross-polarization but not at co-polarization.

Further, we have unambiguously estimated the diameter of the convective rain cells. Figure 3(b), shows line profiles of σ_0 (dB) along the pixel of the C-band SAR at three different cross-sections

corresponding to solid line in Figure 3(a). The solid blue color shows the mean by considering 5 pixels left and right to the each solid line and standard deviation is also plotted in Figure 3(b). The σ_0 cross-polarization (HV) values were found to be around -15 to -25 dB, in the present case. Alpers et al. (2020) also observed a similar range of SAR cross-section values in the presence of a melting layer. From the profile along A2-B2, the σ_0 increased from pixel 200 to 600, and the convective rain cell consists of around 400 C-band SAR pixels. The resolution of each pixel is 50 m. Therefore, the diameter of the convective rain cell estimated from C-band SAR is about 20 km, coinciding with the GPM Ku-band radar value. At A1-B1, and A3-B3, the diameter of the rain cell is estimated to be around 12.5 km and 17.5 km, respectively. From this figure 3, it is evident that the C-band SAR image shows multiple convective rain cells with various diameters. Thus, C-band SAR measurements can be utilized to identify the diameter of the convective rain cores within the mesoscale convective precipitating systems. Hence the present study lies in demonstrating the potential of high spatial resolution of C-band SAR measurements in the detection of signatures of convective rain footprints and providing insights into the small-scale precipitation cells, which are embedded into the mesoscale convective precipitating systems.

4. Summary and conclusions

In the present study, the signatures of convective rain cells are investigated using near-simultaneous observations from C-band SAR onboard the EOS-4 satellite and GPM-GMI and Ku-band precipitation radar for the first time. The following are the summary of the results.

1. The footprints of convective rain cells appeared as bright patches on the C-band SAR image.

2. The bright areas are formed due to the reflections of the C-band SAR backscattered signal from the hydrometeors, such as ice/snowflakes s in the melting layer.
3. The GPM observations confirm the presence of heavy rain rate cells. From the Ku-band precipitation radar, the convective rain core observed that the vertical extent of the cloud was 16.5 km, and the width of the melting layer was around 1.2 km.
4. Estimated the diameter of the convective rain core unambiguously using σ_0 of SAR, and it was found to be around 20 km in the present case, where the GPM Ku-band precipitation radar observed the same to be 22km.
5. Thus, the present study utilizes the near-simultaneous observations from C-band SAR onboard EOS-4 satellite and GPM satellite observations for unambiguously identifying the signatures of convective rain cells.

In future, we will decipher between convective and stratiform rain signatures on C-band SAR imagery and the possibility between C-band backscattered signals with lighting events. Thus, the present study demonstrates the potential of C-band SAR for the signatures of convective rain cells.

Acknowledgements

We gratefully acknowledge the Bhoonidhi portal for making the SAR data publically open. We also thank GPM team for providing the data publically.

Author contributions

Conceptualization: Prakash Chuahan, Kandula V Subrahmanyam. **Analysis and Methodology:** Kandula V Subrahmanyam. **Writing – original draft:** Kandula V Subrahmanyam. **Review & editing:** Rjashree V Bothale, Swapna, Prakash Chuahan.

Competing interests

The authors declare no competing interests.

Data Availability

C-band SAR image data can be downloaded from the Bhoonidhi portal (https://bhoonidhi.nrsc.gov.in/bhoonidhi/index.html#, last accessed on 10 November 2022). The GPM level 2A DPR product can be downloaded from https://storm.pps.eosdis.nasa.gov/storm/.

References

1. Alpers, W., Z. Yuan, A. Mouche, Chan, P.W. 2021. "A note on radar signatures of hydrometeors in the melting layer as inferred from Sentinel-1 SAR data acquired over the ocean" Remote Sensing of Environment 253:112177 (10p.) https://doi.org/10.1016/j.rse.2020.112177
2. Alpers, W., Zhang, B., Mouche, A., Zeng, K., and Chan, P.W. 2016. "Rain footprints on C-band synthetic aperture radar images of the ocean – Revisited." Remote Sensing of Environment 187:169-185. doi.org/10.1016/j.rse.2016.10.015
3. Arakawa, A., The Cumulus Parameterization Problem: Past, Present, and Future, Journal of Climate 17(13): 2493–2525. doi.org/10.1175/1520-0442(2004)017<2493:RATCPP>2.0.CO;2

4. Braun, N., and M. Gade. 2006. “Multifrequency scatterometer measurements on water surfaces agitated by artificial and natural rain.” International Journal of remote Sensing 27:27-39.
5. Browne, I.C., Robinson, N.P. 1952. “Cross-polarization of the radar melting-band.” Nature 170: 1078–1079.
6. Danklmayer, A., B.J. Döring, M. Schwerdt, and M. Chandra. 2009. “Assessment of atmospheric propagation effects in SAR images.” IEEE Transactions on Geoscience and Remote Sensing 47:3507-3518.
7. Fu, L., and B. Holt. 1982. “Seasat Views of the Oceans and Sea Ice with Synthetic Aperture Radar.” JPL Publication 81-120, Jet Propulsion Laboratory, Pasadena, California, pp. 106-107
8. Houze, R. A., Jr. 1997. “Stratiform precipitation in regions of convection: A meteorological paradox?, Bulletin of American Meteorological Society 78:2179 – 2196.
9. Jameson, A.R., and Co-authors. 1997. “SIR-C/X-SAR observations of rain storms.” Remote Sensing Environment, 59, pp. 267-279
10. Mapes, B.E. and R. A. Houze Jr. 1995. “Diabatic divergence profiles in western Pacific mesoscale convective systems.” Journal of Atmospheric Science 52:1807–1828.
11. Melsheimer, C., W. Alpers, and M. Gade. 1998. “Investigation of multi-frequency/multi-polarization radar signatures of rain cells over the ocean using SIR-C/X-SAR data.” Journal of Geophysical Reserach 103:18867-18 884
12. Ouchi, K. 2013. “Recent Trend and Advance of Synthetic Aperture Radar with Selected Topics.” Remote Sensing 5:716-807. doi:10.3390/rs5020716

13. Reihl, H., and J. Malkus. 1958. “On the Heat Balance in the Equatorial Trough Zone.” 503–537. http:// snow.atm.ncu.edu.tw/TC/RiehlMalkus1958.pdf
14. Subrahmanyam, K., and Kumar, K.K. 2020. “The vertical structure of latent heating and its association with cloud types during the Indian summer monsoon.” Remote Sensing Letters, 11:12, 1070-1079, DOI: 10.1080/2150704X.2020.1820615
15. Xu, F., X. Li, P. Wang, and Y.Q. Jin. 2015. “A backscattering model of rainfall over rough sea surface for synthetic aperture radar.” IEEE Transactions on Geoscience and Remote Sensing 53:3042-3054

Table 1: Characteristics of various operation modes of C-band SAR

Operation mode	**Resolution**	**Swath**	**Field of regard**	**Polarisation**
HRS (High Resolution Spotlight)	1 m	10 km	659 km, either right or left	HH or VV or HH/HV or VV/VH
FRS-1 (Fine Resolution Stripmap-1)	3 m	30 km	659 km, either right or left	HH or VV or HH/HV or VV/VH
FRS-2 (Fine Resolution Stripmap-2)	9 m	30 km	659 km, either right or left	VV/HH, HH/HV, VV/VH
MRS (Medium Resolution ScanSAR)	25 m	120 km	659 km, either right or left	HH or VV or HH/HV or VV/VH
CRS (Coarse Resolution ScanSAR)	56m	240 km	659 km, either right or left	HH or VV or HH/HV or VV/VH

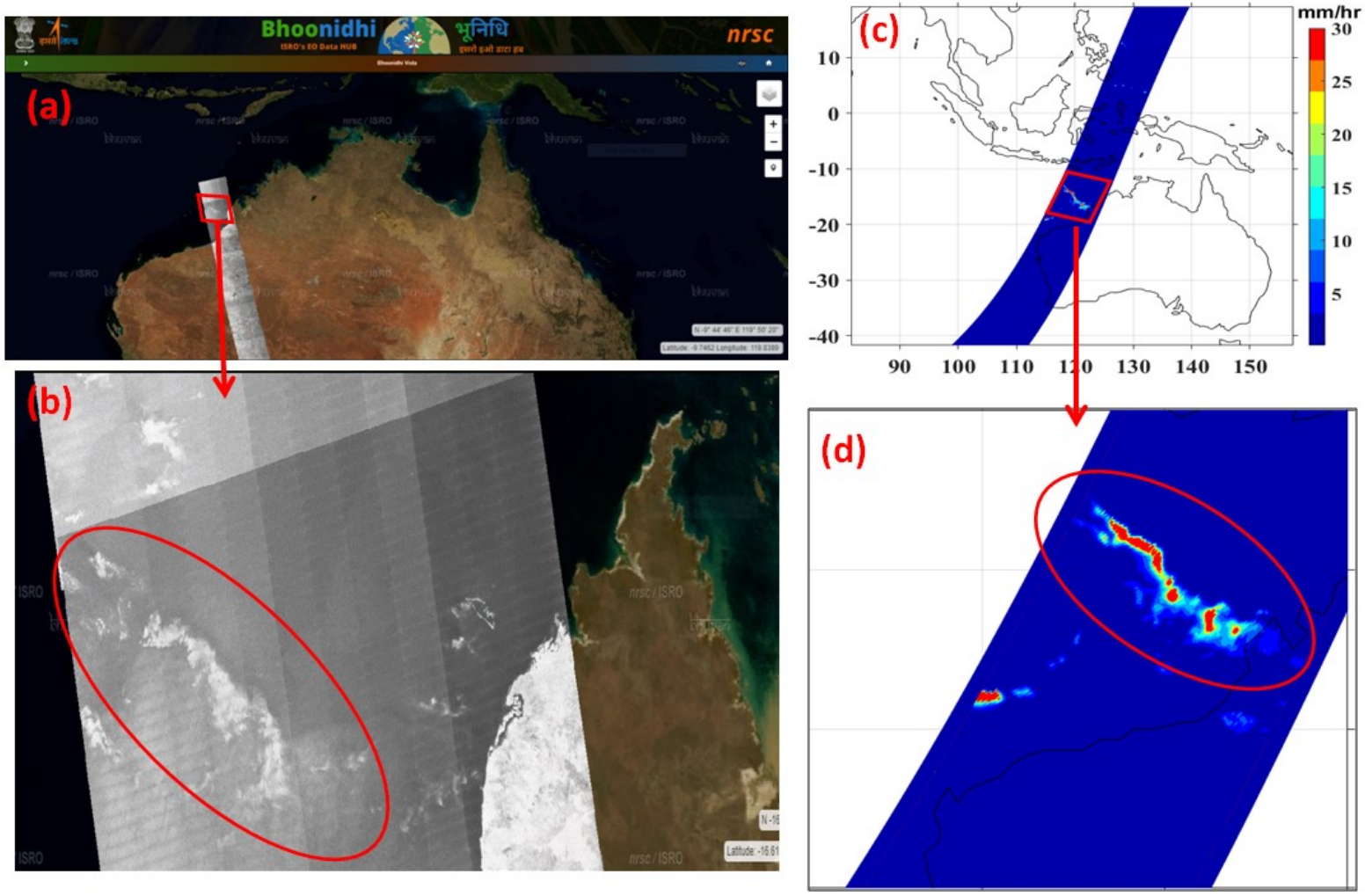

Figure 1: (a & b) C-band SAR image over the Australian Sea coast on 30 May 2022 (c & d) GPM-GMI rain rate

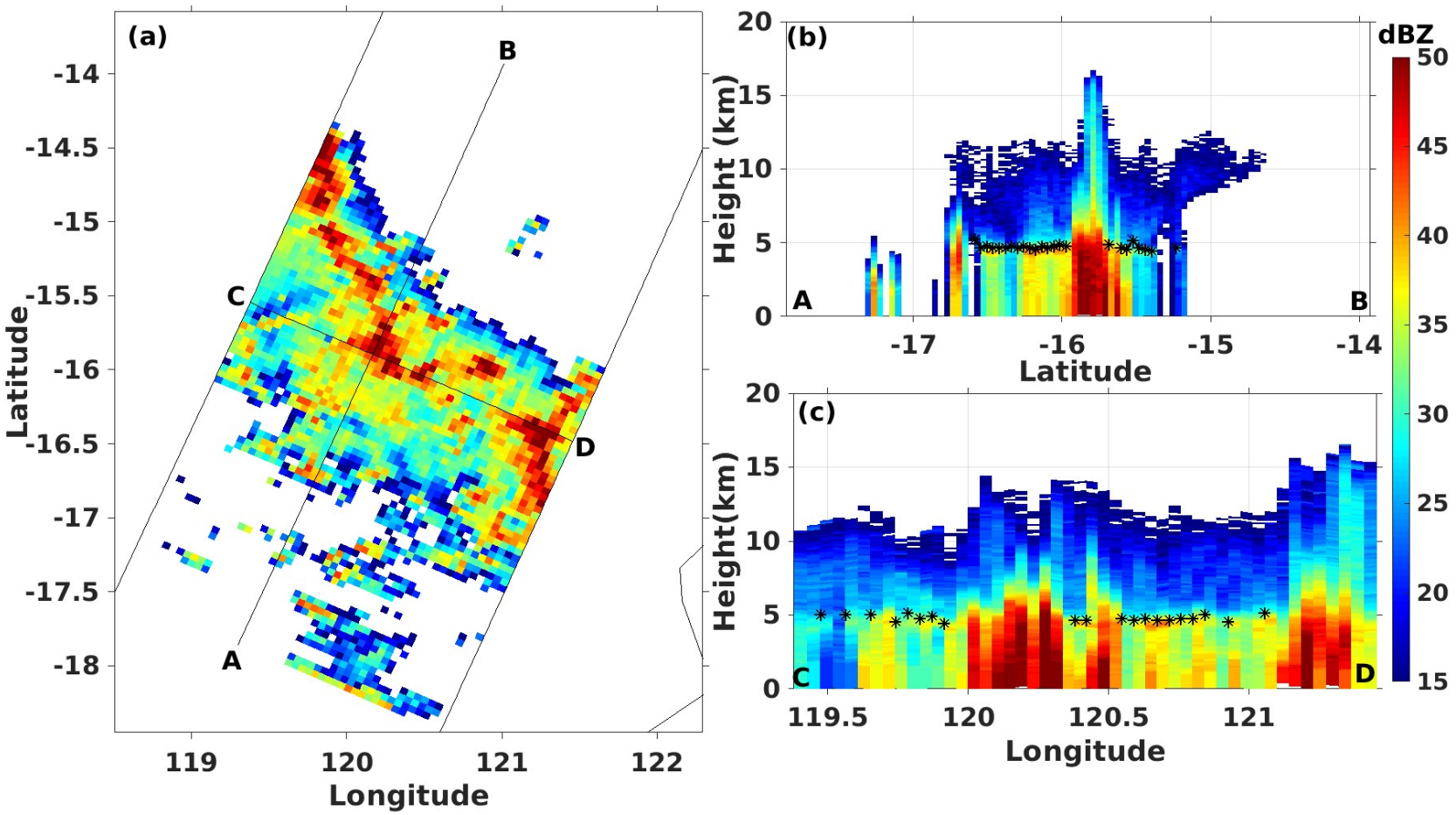

Figure 2: (a) The spatial distribution of reflectivity form GPM Ku-band radar at 2 km height on 30 May 2022 (b) & (c) vertical cross-sections of reflectivity corresponding to solid line AB & CD in (a), respectively. Asterisk symbol denotes the height of melting layer.

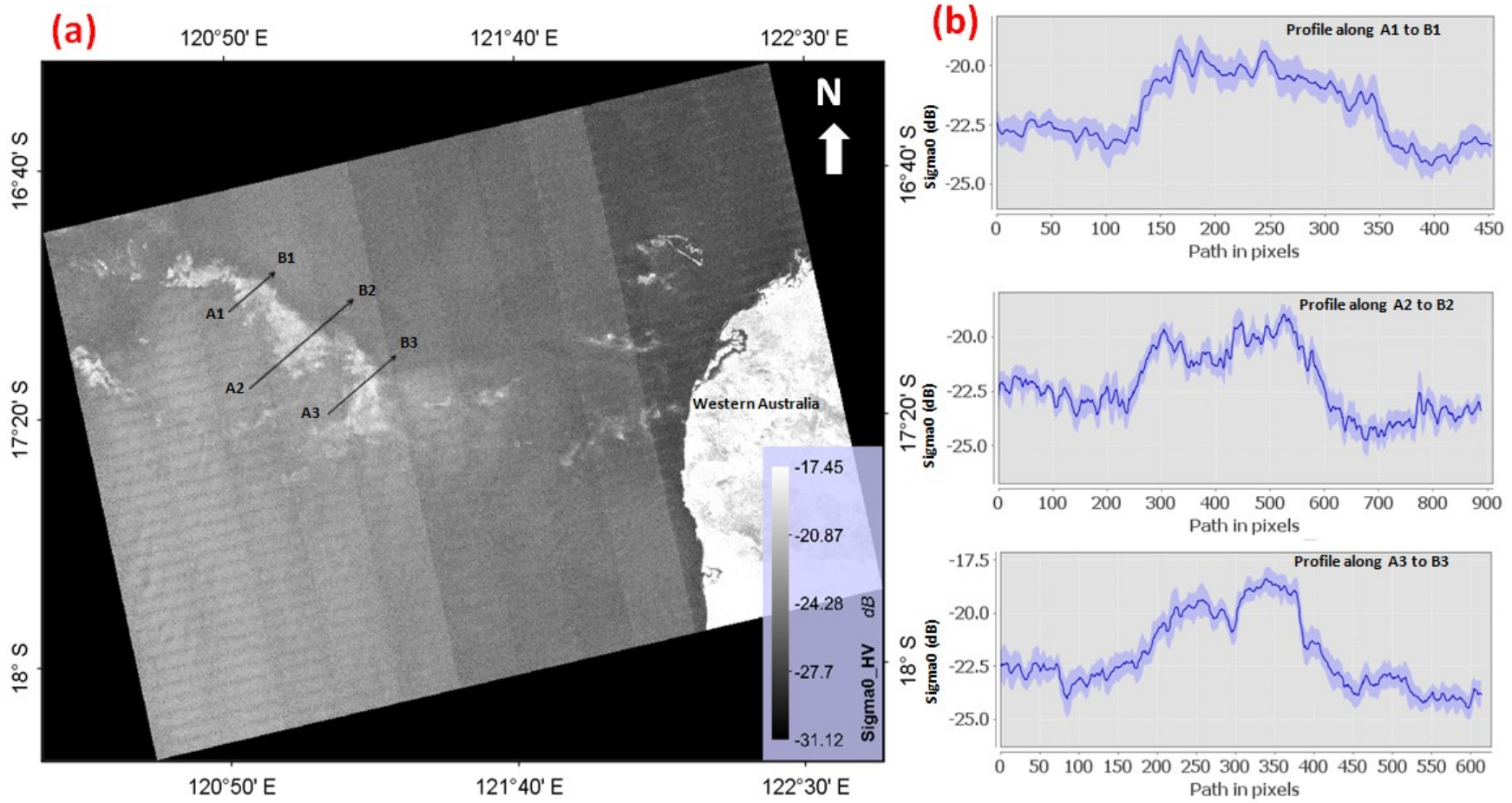

Figure 3: (a) the spatial distribution of σ_0 (b) mean cross-sections of rain cells corresponding to solid lines of A1-B1, A2-B2, & A3-B3 in (a).